VOL. 34, NO. 8, 2025
10.48047/jocaaa.2025.34.08.15

Improvement of image contrast in modeling and optimization of the bubble dimensions in column flotation

Nima jafari [1*], Sead Zia Aldin Shafahi Tonkaboni [1]
1 School of Mechanical Engineering, College of Engineering, University of Tehran, P.O. Box 11155-4563, Tehran, Iran.
*Corresponding Author: nimajafari@ut.ac.ir

Research Highlights

- The contrast of the bubble image has been enhanced.
- The image enhancement and edge detection methods were combined.
- Bubbles carrying minerals were distinguished from those not carrying minerals.
- This information is very useful for discussing intelligent factory control systems.

Abstract

The attachment of particles to bubbles in column flotation is a critical parameter for optimizing mineral processing. This study was conducted in a Plexiglas column (50 mm diameter, 3.5 m height) to address the challenge of poor image visibility due to silica-induced opacity in the middle section of the column. We propose a novel image enhancement method combining Retinex-based, global, and local contrast enhancement techniques to improve the visibility of bubbles and ore particles. The method achieved a 30% improvement in contrast (measured by Peak Signal-to-Noise Ratio) and enabled accurate distinction between bubbles carrying minerals and those without, as validated by edge detection accuracy of 85%. This approach enhances the monitoring and control of flotation parameters, offering a cost-effective solution for intelligent factory systems.

Keywords: Column Flotation Cell, Mineral Processing, Image Enhancement, Retinex-based contrast enhancement, Global contrast enhancement, Local contrast enhancement

1. Introduction

Flotation is the process of separating valuable minerals from useless ones (gangue) by using a differential reaction to air bubbles. The process is carried out in two different types of devices: mechanical cells that use an agitator to hold the pulp in suspension and pneumatic cells that use air to perform the process (Wills et al. 2006). Flotation columns are the most common devices in the latter category. These consist of tall cylindrical vessels that are filled with a slurry of finely ground minerals at an approximate height of 80% (del Villar et al. 2010). Using a sparger device, the air is dispersed from the bottom portion of the device. Moreover, this rise of bubbles contributes to the suspension of particles through their collection. Several spargers are usually used to ensure adequate airflow into the industrial columns. The surface of valuable minerals (metal particles) is usually treated with chemicals in the process of conveying them into the column so that they can attach to the rising bubbles (Galvin, Harvey, and Dickinson 2014). The difference in specific gravity between pulp and bubble-particle aggregates causes the latter to float to the top of the column, forming froth rich in minerals. In most cases, the concentrate overflows the top of the column. Nevertheless, the gangue (generally non-valuable minerals) is discharged through the bottom of the column in a stream called tailing (Wills et al. 2006). Froth plays an important role in determining both grade and recovery. Flotation froth structure plays an important role in

VOL. 34, NO. 8, 2025
10.48047/jocaaa.2025.34.08.15

determining the performance of the flotation process, which has long been known to process operators and researchers (Jera and Bhondayi 2021).

Studies have demonstrated that the bubble size at the froth surface is strongly influenced by the process conditions and the performance of the process (Aldrich and Feng 2000). Several techniques have been developed in recent years for assessing bubble size distribution in froth images in an efficient and rapid manner. Segmentation based on watershed algorithms is one of the most common techniques (Bonifazi et al. 2001; Cipriano et al. 1998; Mehrshad and Massinaei 2011; Sadr-Kazemi and Cilliers 1997), valley edge detection approach (Wang, 5th, and 2000 n.d.) and texture spectrum (Jahedsaravani, Marhaban, and Massinaei 2014). Metallurgical parameters and the status of the flotation process can be estimated using froth optical features, as reported previously in previous publications (Jahedsaravani et al. 2014). As a consequence, image analysis techniques have been developed to measure bubble size, froth velocity, and other characteristics of the froth images (Sadr-Kazemi and Cilliers 1997). For a better understanding of froth characterization, multiple factors should be considered at once, according to studies in this area. Combining mathematical methods is more beneficial than relying solely on one approach. Recently, techniques such as principal component analysis (PCA) and artificial neural networks (ANNs) have been proposed as applications for predictive analysis when the data is complex or when nonlinear effects and interactions are involved (Bonifazi et al. 2001).

Image processing was used by many researchers in order to obtain the most accurate results in the mentioned tasks (Jahedsaravani et al. 2014), which could be referred to as automatic control of mineral processing systems. Due to their time-consuming nature, this type of monitoring and analysis will cause fatigue for the observer, which will result in a higher rate of false conclusions. A further advantage is that image processing systems have a lower cost than other solutions, and they are easier to set up than other solutions. A high level of accuracy is also achieved in the extraction of bubble and particle parameters. Recent studies have focused on the imaging features of certain flotation froths found in both the metals and non-metals industries. The morphology, the colors, and the textures are commonly used as indicators of good performance when recognizing working conditions from froth images (Bonifazi, Massacci, and Meloni 2000, 2002). The GLCM algorithm was proposed by Haralick to define the texture features of an image (Haralick, Dinstein, and Shanmugam 1973). Through the application of GLCM to identify the flotation conditions on froth surfaces, Ren et al. were able to determine the texture of the froth surface (H Ren 2011). A second order NGLDM statistic was used by Sun and Wee to describe the texture of an image (Sun and Wee 1983). In addition to coarseness and roughness, NGLDM has been demonstrated to be a useful tool for describing froth appearance (W Liu 2003; Zhao et al. 2015). Using an improved NGLDM, Peng developed a method for recognizing working conditions during the roughing of antimony (Peng et al. 2016). According to Xu et al., a network-based texture extraction and classification method was developed for mineral flotation froth imaging (Xu et al. 2015). Liu proposed a method of classifying froth size dynamic distribution features based on the relationship between morphology, texture, and froth classification, as well as a classification and recognition method for flotation production conditions using multi-scale and multi-direction texture representations of images for flotation production conditions. In order to perform the classification and recognition of the froth images, a condition recognition model based on the extracted color and texture features of a froth image was developed. Liu recognized flotation production conditions based on the color characteristics of the image of the froth (M Liu 2015).

VOL. 34, NO. 8, 2025
10.48047/jocaaa.2025.34.08.15

The development of technology has made convolution neural networks increasingly useful in the recognition of images, as well as in the recognition of flotation froth images. A convolutional neural network was used by Zarie to classify the froth images of coal flotation fields (Zarie, Jahedsaravani, and Massinaei 2020). Convolutional neural networks were used by Wang to extract morphological features from the froth image, which were then fused with those features to cluster the images (Wang et al. 2020). Three pre-trained convolutional neural networks were used to estimate the froth level on industrial images (namely AlexNet, VGG16, and ResNet), demonstrating the superiority of AlexNet over VGG16 and ResNet (Fu and Aldrich 2020). There is a difference between images of floating froth and natural scenery. There are countless bubbles surrounding mineral particles in froth images, which makes them difficult to identify as they lack a recognizable background or suitable subject or subject matter. The differences between froth images are not readily apparent. Using convolutional neural networks for flotation froth image classification has some limitations, including the requirement to adjust parameters and train large samples over time (Jahedsaravani, Massinaei, and Zarie 2022).

Recent studies have highlighted the importance of bubble size distribution and froth characteristics in determining flotation performance. However, most existing image analysis techniques, such as watershed-based segmentation and valley edge detection, struggle with high opacity caused by fine particles like silica in the middle section of flotation columns. For instance, Haralick's Gray-Level Co-occurrence Matrix (GLCM) and Sun and Wee's Neighboring Gray-Level Dependence Matrix (NGLDM) are effective for froth surface texture analysis but fail to address the haziness in the pulp zone, limiting their applicability for real-time parameter extraction. Similarly, principal component analysis (PCA) and artificial neural networks (ANNs) have been used for predictive modeling, but their reliance on clear input images restricts their use in highly turbid conditions.

The proposed method focuses on the middle section of the column, where bubble-particle interactions are most intense, as this region provides critical data for optimizing flotation efficiency. Unlike froth surface analysis, which is well-studied, the middle section poses unique challenges due to poor visibility caused by high particle concentrations. By combining Retinex-based, global, and local contrast enhancement, our approach overcomes these limitations, enabling accurate detection of bubble and particle features in opaque conditions. This facilitates real-time monitoring and control, addressing a critical gap in existing flotation image analysis techniques.

Research on the identification and classification of froth images has been conducted using supervised and unsupervised machine learning methods, as well as deep learning methods. However, few studies have utilized semi-supervised machine learning for classification and recognition. There are many types of froth that are produced by coal flotation, each possessing multiple properties at the same time. A Gaussian distribution trend is one of its characteristics when there are a sufficient number of froth samples within a given period of time. GMM is an excellent algorithm for detecting patterns in nonlinear, high-dimensional data. In contrast, Gauss mixture models (GMM) belong to the unsupervised learning category. As a consequence of this method, clusters are not visible and must be classified by human judgment. Using a semi-supervised Gauss mixture model (SSGMM) froth image classification method, Wenyan Cao et al. addressed the shortcoming of the Gauss mixture model. A classifier and recognition model for flotation production is important due to the complexity of froth image feature data, the low accuracy of froth recognition and classification, as well as the difficulty controlling reagent dosage accurately. Additionally, froth image classification models need to be developed based on a variety

VOL. 34, NO. 8, 2025
10.48047/jocaaa.2025.34.08.15

of complex and diverse froth image features. The complexity and diversity of froth image feature data necessitate both the collection of better feature data and the development of a model capable of accurately classifying froth images. A combined classification model was proposed for froth image classification to achieve high accuracy. Flotation images of coal are classified using a hybrid classification model (Cao et al. 2022a, 2022b).

The purpose of this study is to provide an overview of basic definitions for image compression, camera specifications, image processing, contrast enhancement (including global contrast enhancement and local contrast enhancement), and Retinex-based enhancement. The results of the experiments on the dataset demonstrate the superior performance of the algorithm. An intelligent algorithm is used to assess metallurgical parameters online and automatically from image data collected during column flotation tests.

2. Image Compression and Camera Readout

In mineral processing, automatic control is often achieved by analyzing the features of froth bubbles at the top of the column. In the middle of the column, bubbles interact with ore particles the most. Unfortunately, the lack of clarity of vision in this section of the column makes it difficult to obtain sufficient input data from the camera for processing. The lack of vision is dependent on the feeding rate of ore particles as well as the type of ore. Image enhancement techniques have been employed to reduce haziness in the image and to enhance the clarity of bubbles and particles. The visibility of details and detection of bubbles and particles in the middle section of the column, which is the main interaction between the bubbles and ore particles, has been improved as a result of this enhancement.

In the first phase of this proposed method, Retinex-based enhancements are used to reduce the low visibility of the image, such as fogginess or blurriness in the background, particularly in the foreground. Following this section, it is expected that the images will show details of the ore particles and bubbles in the water. The result of Retinex-based enhancement is then used as input for a contrast enhancement system. Local enhancement is incorporated into the contrast enhancement system in order to enhance the details of the image in areas that are dark or bright. The resulting image will then be enhanced globally in order to utilize the maximum dynamic range of contrast possible. The purpose of this section is to emphasize the discrimination of bubbles and particles from the background, which in this instance is cloudy water. Analysis of the behavior of different ore particles with different parameters with a wide range of bubbles is an important aspect of flotation systems. Considering that this type of analysis can only be performed in the interaction section for particles and bubbles, which is located in the middle section of the floating system, the existence of such an algorithm will be extremely important.

Mineral processing systems are often fed with particles with a size of a few micrometers. Therefore, the size of particles cannot exceed a few pixels even in high-resolution cameras. There are several problems associated with this situation, including the type of image compression. In addition, high compression rates may result in blockiness and blurriness in image pixels. Specifically, blockiness destroys image details, especially in small objects, and blurriness is likely to produce a smoothness in the image details, which could lead to the loss of small details. The maximum compression rate is determined by the particle size, the distance between the camera and the column, the field of view of the lenses used, and the main characteristics of the camera. By analyzing the distance of the camera to the column and the view field of the camera lens, we can determine the coverage area of the scene by capturing an image of it. By reducing the field of view for camera lenses or reducing the distance between the camera and the column, objects and

VOL. 34, NO. 8, 2025
10.48047/jocaaa.2025.34.08.15

details could appear larger than normal (like zooming) however, the area covered by the column in the captured scene will also be reduced. Therefore, obtaining optimal area coverage and details will require solving a tradeoff problem.

There are two main types of compression. The first type of compression is lossless compression, which encodes an image without causing the data of the captured scene to be lost. Another type of encoding is lossy, which reduces the file size of the image while maintaining the quality of the image. Thus, it is much better to choose lossless compression methods or more effective lossy compression methods rather than choosing a compression method. In the ideal case, video frames captured from a camera should not be compressed in any way.

3. Camera Specification

The selection of the appropriate camera can have a substantial impact on the input data / captured frames. The following parameters may be considered when selecting a camera: resolution, frame rate, field of view, and dark noise. A camera's resolution indicates how many photodiodes are necessary to construct each frame of video. The frame rate of a camera indicates how many frames can be captured within a second. The angle of view for integrating a camera sensor and lens package is demonstrated by the field of view for a camera. The field of view is defined as the amount of length and height that the camera sensor will be able to capture at any given distance from the camera. A camera's dark noise determines how noisy an image will be captured at low luminance levels. Proper lighting conditions can be used to overcome this type of noise. The higher the resolution, the more detail will be captured. Conversely, this higher resolution will require more computation time in the image processing system. In a smaller field of view, a smaller portion of the column area is received, and in a larger field of view, more portions are received. Accordingly, the right field of view will consist of just the entire column width that the camera is focusing on. In addition to allowing us to track changes in mineral processing system parameters more effectively, high frame rates will also result in more noise in the frames due to the lower shuttering time of the camera. Cameras with smaller dark noise are always preferred for dark noise reduction. The choice of camera is ultimately left to the discretion of the researcher.

3.1. Image Processing

Photodiodes used in visible camera sensors are sensitive to visible wavelength illumination. The output voltage of each photodiode in the output image is affected by changes in the illumination of the scene. Each photodiode represents a pixel in the output image of the camera. An analog-to-digital converter (ADC) will be used to measure all photodiode voltages. Depending on the resolution of the ADC, the digital output can be a specific amount. For example, the readout of the analog voltage of photodiode for 8-bit / 12-bit / 16-bit ADC could be respectively in 2^8 / 2^{12} / 2^{16} possible specific states. Most cameras use an 8-bit ADC, which means that each pixel in the output image can be characterized in 256 different ways. A number of pixels are assigned a number between 0 and 255 (256 different states) that indicates their illuminance due to the simplicity of image processing. Instead of using exact quantized voltage, each pixel is assigned a number between 0 and 255 (256 different states). It is established a 2D matrix of numbers between 0 and 255 by concatenating the data of each pixel. Image processing algorithms use this matrix as the input for their illumination intensity algorithms.

3.2. Contrast Enhancement

VOL. 34, NO. 8, 2025
10.48047/jocaaa.2025.34.08.15

To understand contrast enhancement, it is necessary to understand the meaning of contrast itself. Contrast is a key component of any subjective assessment of image quality. Contrast is created when two surfaces reflect different levels of luminance from each other. As a result, contrast describes the difference in visual properties that make an object stand out from other objects and the background. Visual contrast is defined as the difference in color and brightness between two objects. Due to the fact that the visual system is more sensitive to contrast than absolute luminance, it is able to perceive the world regardless of the considerable variations in illumination conditions. As a formula for luminance contrast, the Weber contrast is most commonly used as shown in Eq. 1.

$$\frac{I_s - I_b}{I_b} \quad \text{(Eq. 1)}$$

Where I_s is the luminance of the object and I_b is the luminance of the adjacent background. Increasing the luminance difference will increase visibility and contrast between adjacent areas, as previously discussed.

Many researchers have been working on contrast enhancement (Celik 2012; Srinivas, Bhandari, and Singh 2020) to increase the difference in luminance between adjacent areas and pixels. There are two main categories of contrast enhancement algorithms. Global contrast enhancement and local contrast enhancement are two categories of contrast enhancement. Global contrast enhancement requires a single contrast map, histogram, or function to represent and analyze each image, while local contrast enhancement divides the image into sub-images or patches and analyzes each patch separately.

3.2.1 Global Contrast Enhancement

Global contrast enhancement algorithms calculate image contrast by considering the luminance values of all pixels. The distribution function of the luminance intensity of pixels is one of the most important parameters in global contrast enhancement. There is a function called image histogram that indicates the probability of occurrence for each intensity value among the pixels of an image. A linear equalized function is the ideal type of distribution in which the minimum is equal to the minimum dynamic range (means zero) and the maximum is equal to the maximum dynamic range (means 255). The first step in the contrast enhancement algorithm is to ensure that the full dynamic range is utilized. This fact can be interpreted as follows: To maximize the dynamic range of contrast in an enhanced image, the minimum luminance intensity should equal 0 and the maximum luminance intensity should equal 255. Secondly, it is important to redistribute luminance intensity levels according to their importance in image details. In simple terms, if the probability of occurrence of an intensity level is 0, then it has no effect on the image and should be removed from the new distribution. A high probability of an intensity level is an indicator that it is important and should have a higher contrast than other intensities.

3.2.2 Local Contrast Enhancement

One of the main problems with global contrast enhancement is that parameters and redistribution are calculated based on all pixels of the image. Thus, darker or brighter sections of an image cannot be enhanced in terms of detail. The main cause of this phenomenon is the use of the full dynamic range of contrast when analyzing the histogram of all pixels. It is expected that the details in the dark section of the image will be less visible in an enhanced mode based on global contrast enhancement. Similarly, this section will become brighter than it was previously.

VOL. 34, NO. 8, 2025
10.48047/jocaaa.2025.34.08.15

Therefore, no details would be visible in any of these sections. To achieve enhanced maps or distributions of intensity levels, local enhancement techniques would separate the image into small patches, and global contrast enhancement techniques would be applied to each patch independently. As a result, in order to reduce the artifacts, interpolation will be applied based on the distance between the center of each pixel and the center of the adjacent patches in order to obtain the main enhanced image.

3.3 Retinex-based image enhancement

Retinex-based image enhancement is a popular method for enhancing low-visibility images captured in poor lighting conditions. The term Retinex is used to describe the concept of capturing an image in a form in which a human being perceives it after viewing an object with their retina (Human Eye) and cortex (Mind). In accordance with Retinex theory, an image can be defined as the product of illumination and reflection from an object. Due to Retinex's focus on dynamic range and color constancy, most details should be able to be extracted from the input image in low visibility and unclear circumstances. Retinex-based image enhancement could be used even in foggy or hazy conditions (Liu et al. 2021; Parihar and Singh 2018).

3. Proposed Method

A schematic of the proposed method sequence has been provided for a better understanding of the method in Fig. 1. There are three main subsections of the algorithm. The first subsection is a Retinex-based enhancement section that estimates the true illumination of RGB (color) image frames captured from a camera. Through this estimation, it is possible to understand the details of an image in different parts and enhance them so that they are more visible. Due to low visibility images such as dehazing / defogging problems, unusually bright images have been observed (usually more than usual). Adaptive gamma correction was employed in order to resolve this issue. To maximize the dynamic range of contrast, a global contrast enhancement is used for adaptive histogram stretching. As a final step, local contrast enhancement was employed to obtain details of darker and brighter sections of the enhanced image.

Retinex-based image enhancement decomposes the entire color image into two components: reflectance and illumination. One of the most important factors is the illumination component that determines the solution for the reflection component, which is based on the Retinex model described in Eq. 2:

$$L = R \circ T \quad \text{(Eq. 2)}$$

Assume that L and R represent the captured image and the desired recovery, respectively. Furthermore, T represents the illumination map, and the operator ◦ means multiplication at the element level.

One of the first color constancy methods, Max-RGB (van de Weijer, Gevers, and Gijsenij 2007) attempts to estimate illumination by seeking the maximum value of three-color channels, namely R, G, and B. However, this estimation can only increase global illumination. It is shown in Eq. 3 that illumination maps can be used to handle non-uniform illuminations by estimating the maximum of R, G, and B for each pixel of the image.

$$T(pixel) = Max\ (L^c(pixel)), \qquad c \in (R, G, B) \quad \text{(Eq. 3)}$$

VOL. 34, NO. 8, 2025
10.48047/jocaaa.2025.34.08.15

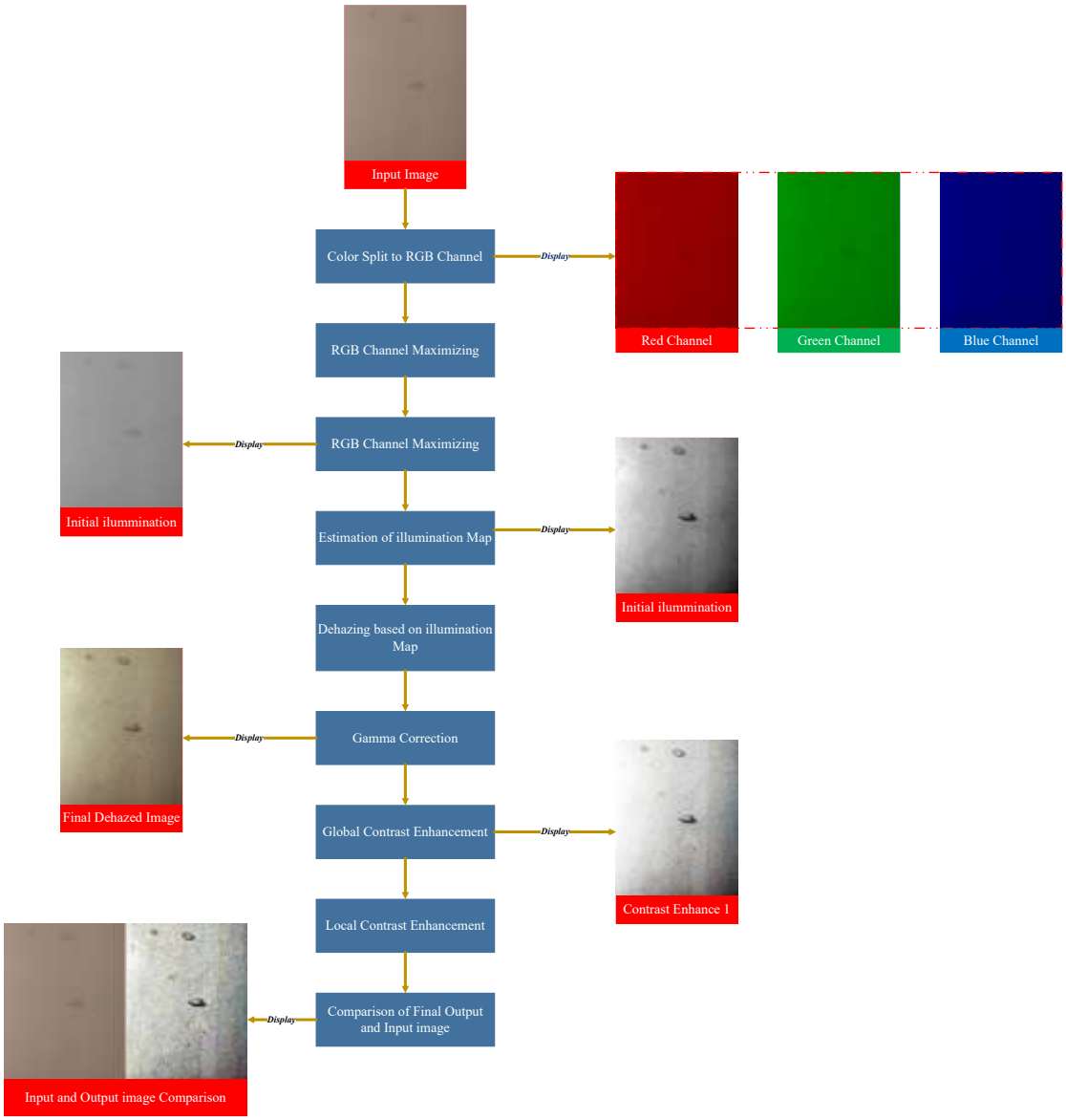

Fig. 1. Proposed method schematic.

Based on Eq. 4, this formula will ensure that the reflection map will not saturate.

$$R(pixel) = \frac{L(pixel)}{Max\ (L^c(pixel) + \varepsilon)} \quad \text{(Eq. 4)}$$

where ε is a very small constant to avoid the zero denominators. This work aims at improving the illumination of low-light images without eliminating the color shift caused by light sources.

It is common to interpret low visibility images as inverses of hazy images, which are discussed in Eq. 5:

$$1 - \mathrm{L} = (1 - \mathrm{R}) \circ \tilde{\mathrm{T}} + \alpha(1 - \tilde{\mathrm{T}}) \quad \text{(Eq. 5)}$$

Where α represents the global atmospheric light that in the method considers 0.95. $1 - \mathrm{L}$ will be the inverse of a low visibility image similar to a haze image, and 1- R will be the total measured volume of the reflected component of the (detailed image) haze image. Solving Eq. 6 results in a detailed image which can be used as input for other subsections of the enhancement process.

VOL. 34, NO. 8, 2025
10.48047/jocaaa.2025.34.08.15

$$R(pixel) = \frac{L(pixel) - 1 + \alpha}{(1 - \frac{1}{a} + \max_c \frac{L^c(pixel)}{a} + \varepsilon)} + (1 - a) \quad \text{(Eq. 6)}$$

The best method of solving Eq. 6 for a complicated scene with many objects with a wide range of illumination or reflectance changes is to solve a recursive sequence to obtain the optimal illumination map. For applications involving water, bubbles, and ore particles (a simple scene with a limited number of objects), complicated mathematics is not required to solve the illumination map. Rather, the illumination map is generated by using a median filter that considers homogeneous illumination and equal distribution of ore particles in the column area. The main formula used in the application is shown in Eq. 7:

$$T(pixel) = |Median_{2D}(\max(L^c(pixel), k)| \quad \text{(Eq. 7)}$$

k indicates the filter area around the central pixel of the image. As a means of adjusting the intensity of the output image and improving visibility after applying the illumination map to the input image, gamma correction is applied according to Eq. 8.

$$T_{final}(pixel) = T(pixel)^{gamma} + \varepsilon \quad \text{(Eq. 8)}$$

4. . *Intensity*

As backgrounds and brightness of captured scenes from column floatation are usually greater than average, tuning the gamma parameter can be used for almost all captured frames. Image produced in this section serves as the main input for enhancing global contrast and enhancing local contrast (lowpass filters can be applied to sequences of estimated illumination maps to reduce noise or uncertainty during illumination map estimation if we have a video or sequences of frames).

At the beginning of the global contrast enhancement process, the entire dynamic range is used to enhance the contrast in the image. An efficient histogram stretching method was employed in order to achieve this goal. This method calculates the maximum and minimum intensity of an input image based on the minimum size of an object, such as bubbles or particles, that is meaningful to the image. Thus, the minimum number of occurrences for representing the smallest object in a scene should exceed the deterministic number. By using this technique, the presence of noise in the image is minimized so that the full dynamic range of contrast can be utilized. In Eq. 9, 10, and 11 are outlined the formulas for the estimation of minimum intensity, maximum intensity, and new intensity map, respectively.

$$Intensity_{min} = \frac{Row \times Col}{Thr} \quad \text{(Eq. 9)}$$

$$Intensity_{max} = \frac{Row \times Col}{Thr} \quad \text{(Eq. 10)}$$

$$Intensity_{Stretch} = 255 \times \frac{(intensity_{origin} - Intensity_{min})}{(Intensity_{max} - Intensity_{min})} \quad \text{(Eq. 11)}$$

It should be mentioned that for intensities lower than $Intensity_{min}$, the new intensity would be 0, and for intensities higher than $Intensity_{max}$, the new intensity would be 255. Otherwise, the new intensity map for pixels will be calculated using Eq. 11.

Creating a new intensity map based on the importance of each intensity is another important aspect of global contrast enhancement. It is expected to have the most contrast for the most

VOL. 34, NO. 8, 2025
10.48047/jocaaa.2025.34.08.15

important intensities and the least contrast for the lesser important intensities. Intensity importance can be determined by the number of occurrences of a particular intensity over the entire image.

The greater the number of occurrences, the greater the PDF in the histogram function. Intensity PDF has a weakness in terms of producing new intensity maps. There should be a PDF greater than half for the intensity of a large homogeneous object in the scene that is larger than half of the entire image size. Therefore, half of the contrasting dynamic will be dedicated to object intensity, while other objects and details will have less contrast. The problem is that a large volume of contrast will be assigned to a homogeneous part of an image that contains small details, and the small details in the image will disappear, which may contain important information. This feature has been limited based on Eq. 12, 13, 14, and 15 in order to prevent this from occurring. Using this technique, the amount of PDF is modified according to the value of the PDF. In the case of higher amounts of PDF, there are more decreases seen, and in the case of lesser amounts of PDF, there are fewer decreases seen.

$$pdf_{old} = \frac{Intensity_{count_{old}}}{Total_{count_{old}}} \quad \text{(Eq. 12)}$$

$$Intensity_{count_{new}} = Intensity_{count_{old}}{}^{\gamma} \quad \text{(Eq. 13)}$$

$$\gamma = \frac{1}{e^{pdf_{old} \times k}} \quad \text{(Eq. 14)}$$

$$pdf_{new} = \frac{Intensity_{count_{new}}}{Total_{count_{new}}} \quad \text{(Eq. 15)}$$

In which γ is the power to decrease values of histogram bins based on their values. This adjustment should be applied to all intensities in the bins of the histogram, and a new summation should be calculated for each new bin to determine the exact new PDF that will be used for producing the new intensity map.

Based on the adjusted PDF, create a new intensity map highlighting the importance of each intensity. For this goal, Eq. 16 and 17 are given.

$$cdf_{new} = \sum_{i=0}^{255} pdf_{new} \quad \text{(Eq. 16)}$$

$$Intensity_{new} = 255 \times cdf_{new} \quad \text{(Eq. 17)}$$

A major problem in global contrast enhancement is making dark parts of images darker and bright parts of images brighter. This would result in a loss of detail in these parts of the image. To resolve this problem, local contrast enhancement was employed, which would split the image into smaller, independent sub-images that would be enhanced individually. The assumption is that the sub-images are small enough to contain only the dark or bright portions of the image. In addition to redistributing intensity maps for each sub-image, gamma correction is used to improve detail visibility in darker or brighter portions of the image.

A CLAHE contrast enhancement is used in contrast enhancement of sub-images (clipped limit adaptive histogram equalization) that limits the maximum PDF of each intensity to a specific number and shares it with all other intensities. However, in the proposed method, limit values are calculated independently for each sub-image. This means that each sub-image has its own unique value and enhancement level. Among the most important factors that determine the level of enhancement is the distribution of the intensity of the pixels within the sub image. An enhancement

VOL. 34, NO. 8, 2025
10.48047/jocaaa.2025.34.08.15

level should be set at a low level if the sub-image contains a homogeneous area that has minor details and a change in intensity levels, such as just the background. In contrast, the enhancement level should be high for sub-images with different intensity levels that contain details. Eq. 18, 19, and 20 are used to calculate enhancement levels in order to reach this goal.

$$Limit = offset + k \times HB_{count} \quad \text{(Eq. 18)}$$

$$HB_{count} = \sum Modified_{Histogram} \quad \text{(Eq. 19)}$$

$$Modified_{Histogram} = \begin{cases} 0 & if\ Histogram_{value} < Histogram_{Limit} \\ 1 & if\ Histogram_{value} \geq Histogram_{Limit} \end{cases} \quad \text{(Eq. 20)}$$

That $offset$ is a constant value for all sub images and $Histogram_{Limit}$ is minimum amount of histogram bin to consider it as part of detail in sub image.

After enhancing all the sub-images, bilinear interpolation was used to overcome discontinuities between the intensity maps of each of the sub images. As a result of the proposed method, the interpolated image would be the final image that could be compared to the input image for the purpose of improving visibility.

5. Materials and methods

5.1. Sample and Characterization studies

Laboratory experiments were conducted on a Silica ore from Kaveh Glass Industrial Group. This silica is prepared from the mines of Abhar city. The required sample was crushed in the first stage with a jaw crusher, in the second stage with a conical crusher (hydrocon) and in the third stage with a washing sieve, and finally reached d80 ¼ 300 microns using a rod mill.

The proposed image enhancement method integrates three stages: Retinex-based enhancement, global contrast enhancement, and local contrast enhancement. The Retinex algorithm, implemented as a multi-scale Retinex with color restoration (MSRCR), reduces haziness by modeling illumination and reflectance components, as described by Jobson et al. (1997). The algorithm uses Gaussian kernels with scales of 15, 80, and 250 pixels to separate low-frequency illumination from high-frequency reflectance, improving visibility in turbid conditions. Global contrast enhancement employs histogram equalization to maximize the dynamic range, using the following transformation for intensity (I):

$$\frac{h(k)}{N} \sum_{k=0}^{I} \cdot 255 = {}_{\text{out}}I$$

where (h(k)) is the histogram of intensity (k), and (N) is the total number of pixels. Local contrast enhancement uses Contrast-Limited Adaptive Histogram Equalization (CLAHE), with clip limits calculated dynamically for each sub-image (8x8 tiles) based on intensity variance, as follows:

$${}^{2}\sigma \cdot \alpha = \text{ClipLimit}$$

Here, α is a constant parameter (fixed at 0.03), and σ2 represents the variance of pixel intensities within the sub-image. To ensure smooth transitions between adjacent sub-images and to minimize visual artifacts, bilinear interpolation is employed.

VOL. 34, NO. 8, 2025
10.48047/jocaaa.2025.34.08.15

5.2. Column Flotation

Laboratory experiments were conducted using a Plexiglas column (50 mm diameter, 3.5 m height) to develop a soft-sensor model for image processing. The column was continuously fed with a pulp containing 10–40% solids (particle size: 10–100 μm). Silica ore (d80 = 300 μm) from Kaveh Glass Industrial Group, sourced from Abhar city mines, was prepared through sequential crushing (jaw crusher, conical crusher) and milling (rod mill). For each experiment, 5 kg of silica was mixed with 60 liters of water in a 100-liter polyethylene container using a mechanical stirrer at 80 rpm for 5 minutes. Armac C (1 g/kg silica) was used as the collector, and methyl isobutyl carbinol (MIBC, 0.5 g/kg silica) was added as the frother, mixed for 2 minutes. The pulp was pumped into the column, and aeration was initiated at a flow rate of 0.2 L/min using a sparger at the column base. After 5 minutes of stabilization, high-speed video was recorded for 2 minutes using a Sony PXW-FS7 camera. Test conditions, including aeration rate (0.1–0.3 L/min) and reagent dosages, were varied to assess their impact on bubble size and distribution.

5.3. Control system and equipment location

This section deals with the structure of cells and equipment related to the control of management variables, sensors, equipment for conversion, amplification and transfer of data to the processor of the processor system, equipment for transfer and conversion of commands to operators, actuators and operators, and finally the monitoring system.

Using designed software, the system is allowed to enter new information every second. The commands issued after the data is processed by the processor and determined by the fuzzy software need to be modified to be applied to the operators so that they can be understood by the operator. For this purpose, intermediaries are needed to perform these command transformations in them, which is done through designed electronic circuits. The actuator part of the control system consists of two parts, the actuator and the final element. In fact, operators are used to control or apply optimal management on management variables. In this system, according to different parts and the type of management variable, different operators have been used, which will be described below.

A. Feed - In this part, a peristaltic pump is used as the final element and an electric motor is used as an actuator which is controlled by a motor speed controller.

B. Fine - This part is also similar to the operators of the feed part.

C. Washing water - In both parts of the washing water section, manual operators are used and in fact in this part only the final element is used as the operator.

D. Bubble supply - Due to the different sections of this part, the final elements and various stimuli play a role in it. In the first part, in fact, a magnetic valve (to cut off and connect the air flow) is a stimulus, which of course can be a final element in its kind. This magnetic valve through an independent command that receives from the controller software.

In order to apply the settings and view the changes applied, a graphical interface is required in the cell through which the above operations can be performed. For this purpose, a monitoring system was designed for this system (Fig. 2) through which the following can be done: 1- Manually turn on or off each power tool. 2- Schematic view of the cell 3- Observation of changes related to floor depth, pulp height, gas retention, foam density, pulp density, and air pressure. 4-Ability to apply changes manually in the pumping rate of each peristaltic pump.

VOL. 34, NO. 8, 2025
10.48047/jocaaa.2025.34.08.15

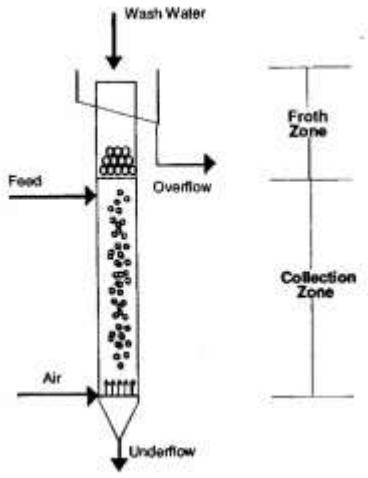

Fig. 2. Schematic view of the level of the installed tool.

5.4. Images acquisition

Image acquisition was conducted using a digital color camera Sony PXW-FS7 cinema camera for high fps video recording. Also, Sachler tripod, LED light on camera, monitor on camera, LED light 1260 with stand, circular SMD light with stand, video reflector, camera metabox, Zeiss 85mm lens, and 50mm Canon are used.

Lighting was supplied by two SMD lights were placed in front of the camcorder and a 1260 LED grid at a 90-degree angle to the camera. Also, all around the cell was completely isolated in a way that no external light could be inserted which showed in Fig. 3. The camera was mounted at 1080P with an 85mm lens and a dynamic range of 10, and the video was recorded on an XQD memory card. This movie reached 960 fps with the help of Twixtor software. In this study the most significant froth characteristics consisting of bubble size, color, texture, bubble collapse rate, and froth velocity were extracted in each test.

Fig 3. Column flotation set-up.

6. Results and Discussion

MATLAB code has been developed for the proposed method on a computer with a clock speed of 4.2 GHZ and a memory capacity of 16 GB. Implementing code for each frame takes approximately 0.4 seconds (average). Obviously, all images were not used. Instead, they were

VOL. 34, NO. 8, 2025
10.48047/jocaaa.2025.34.08.15

cropped based on a region of interest that contained column floatation data. The algorithm has been tested and qualified using a large dataset. Although there are some quantitative metrics that can be used to score the performance of enhancement algorithms, for the most part, human vision is the best method of comparing input and output image details. To compare and qualify the proposed method, many different images were presented with different aspects of detail. Fig. 4 illustrates some of the input images and their enhanced versions. All input images have been presented in the left-hand side of the image and their corresponding enhanced images have been presented in the right-hand side of the image.

(A)

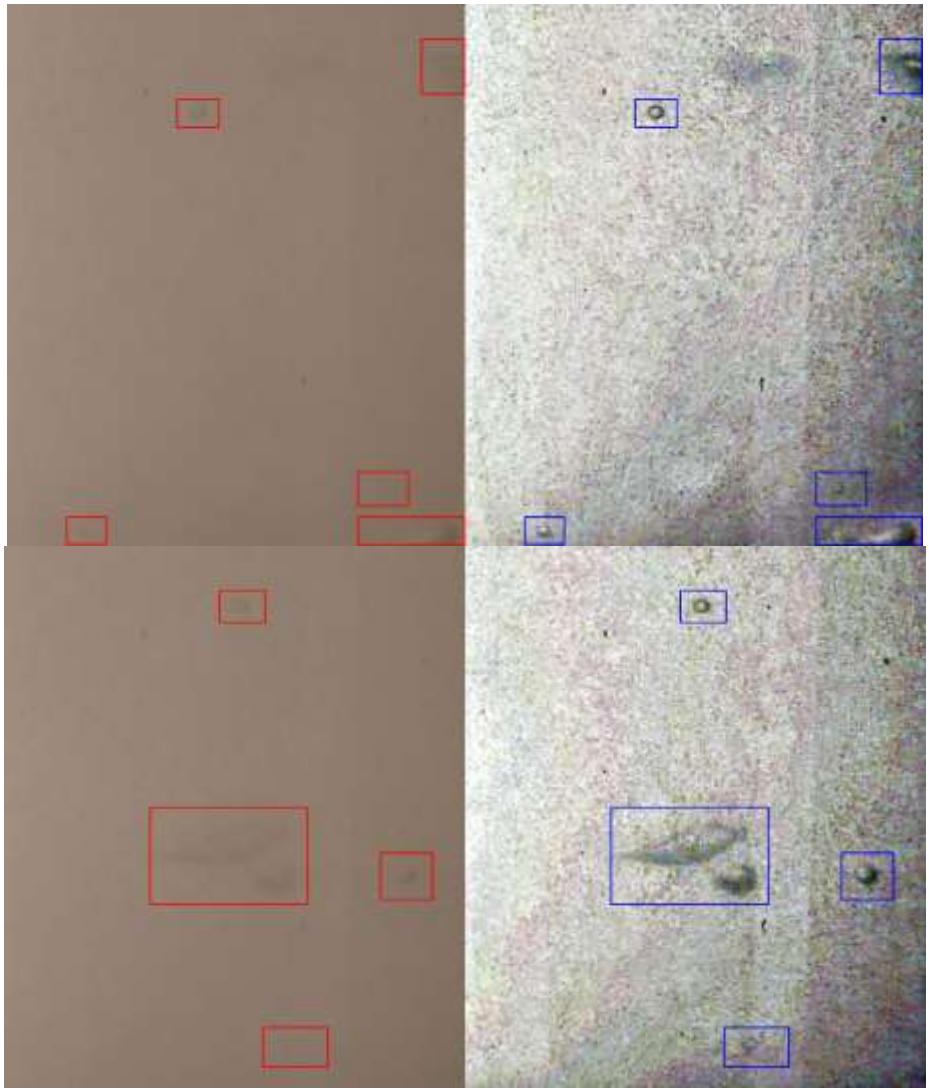

VOL. 34, NO. 8, 2025
10.48047/jocaaa.2025.34.08.15

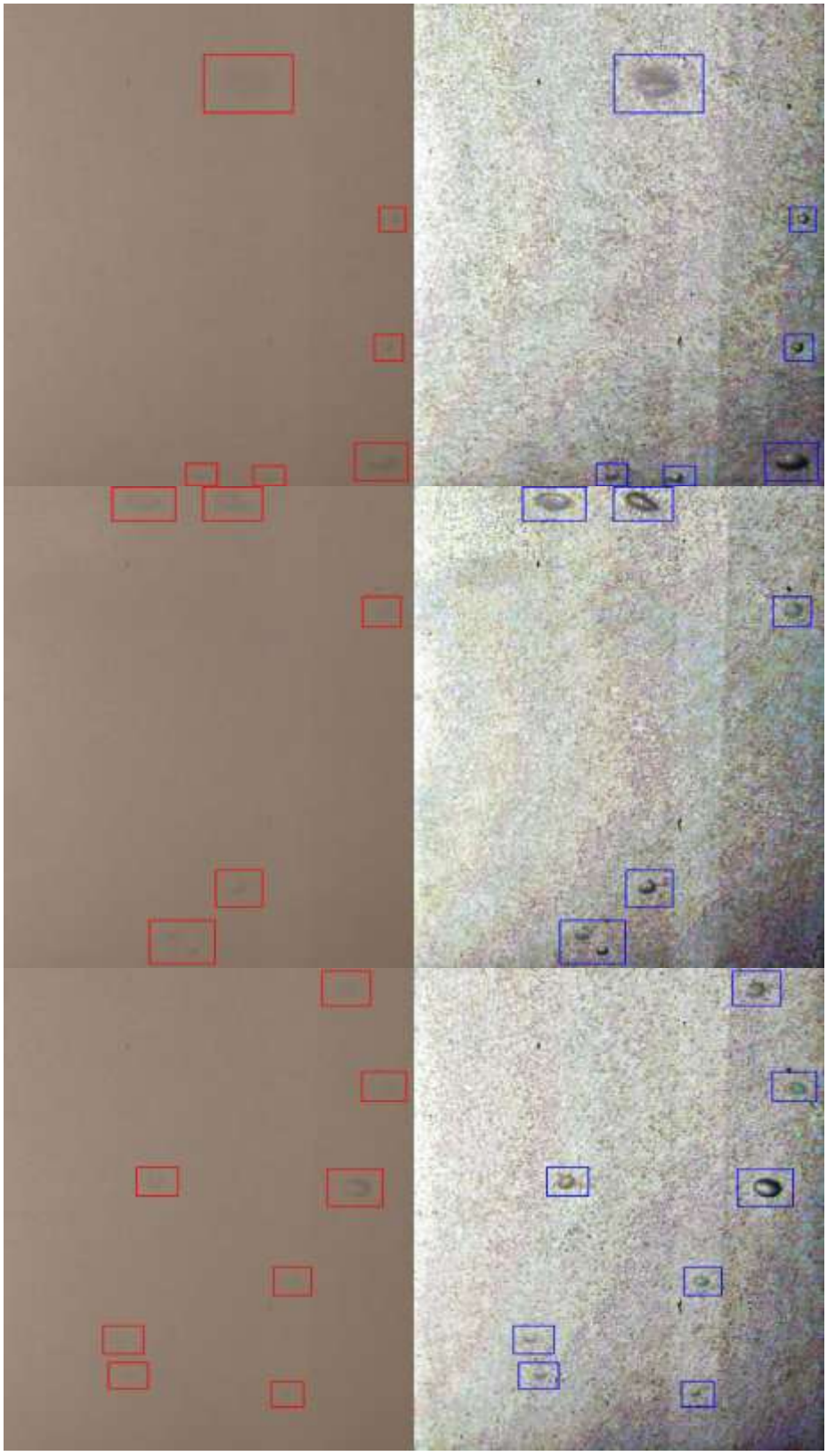

VOL. 34, NO. 8, 2025
10.48047/jocaaa.2025.34.08.15

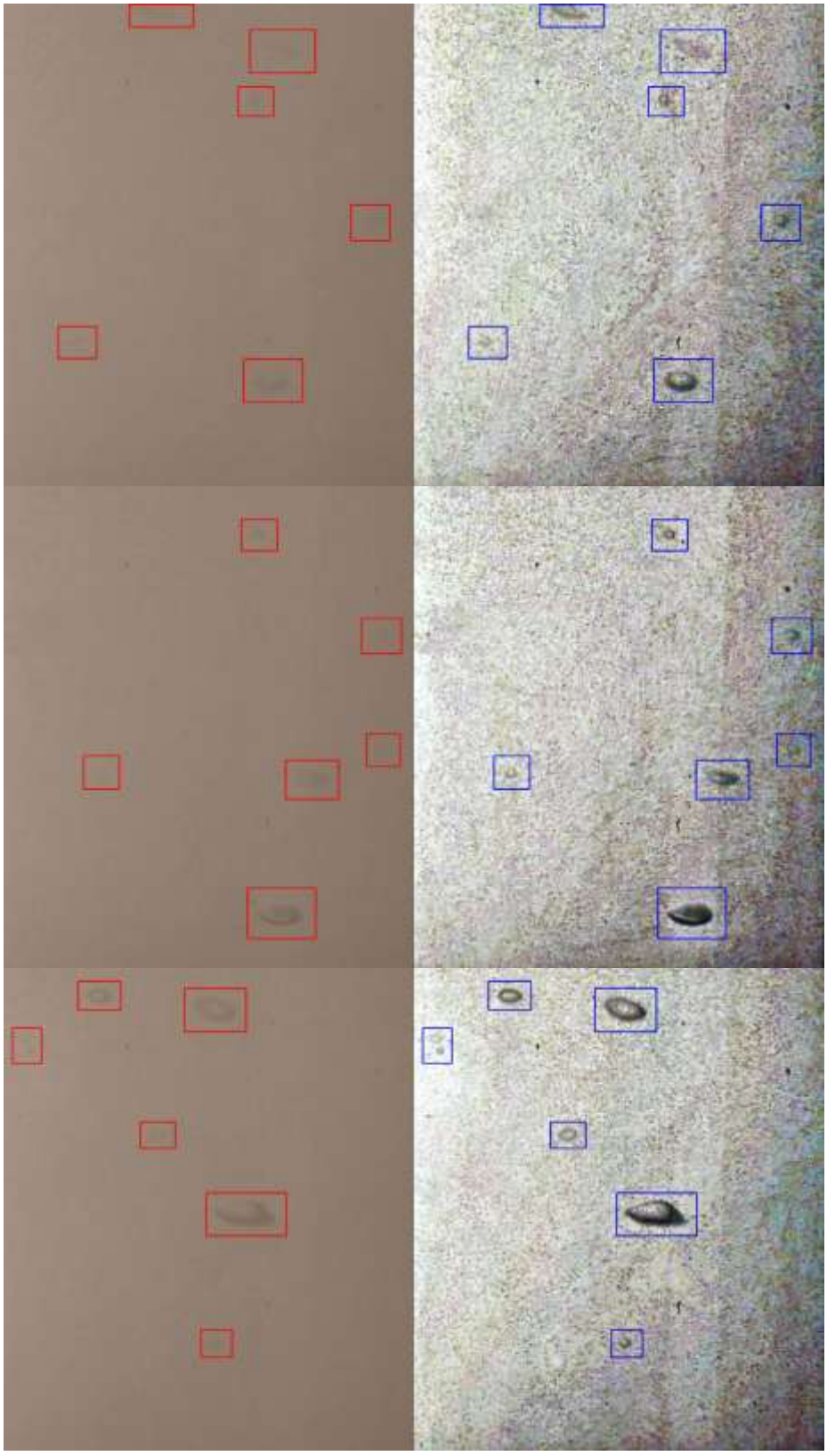

VOL. 34, NO. 8, 2025
10.48047/jocaaa.2025.34.08.15

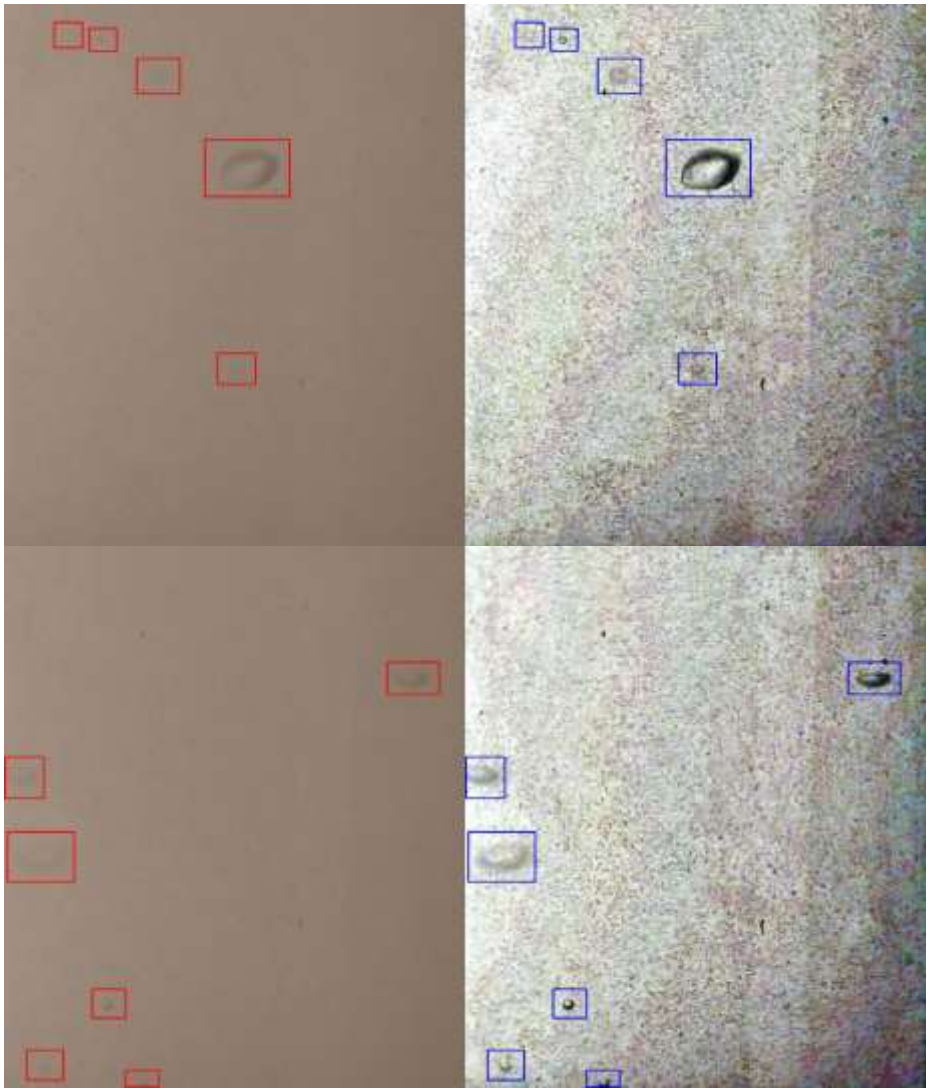

(B)

VOL. 34, NO. 8, 2025
10.48047/jocaaa.2025.34.08.15

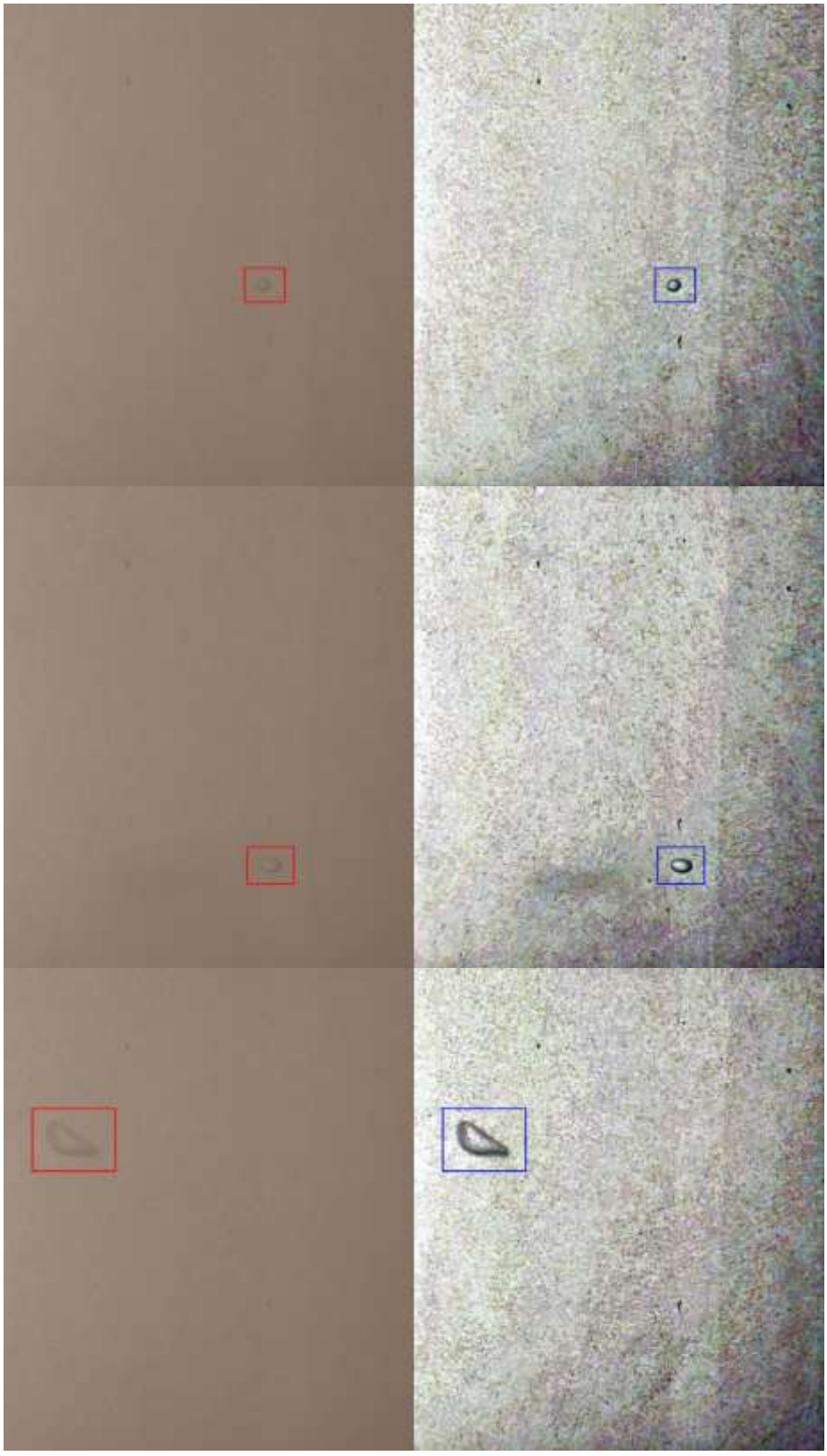

VOL. 34, NO. 8, 2025
10.48047/jocaaa.2025.34.08.15

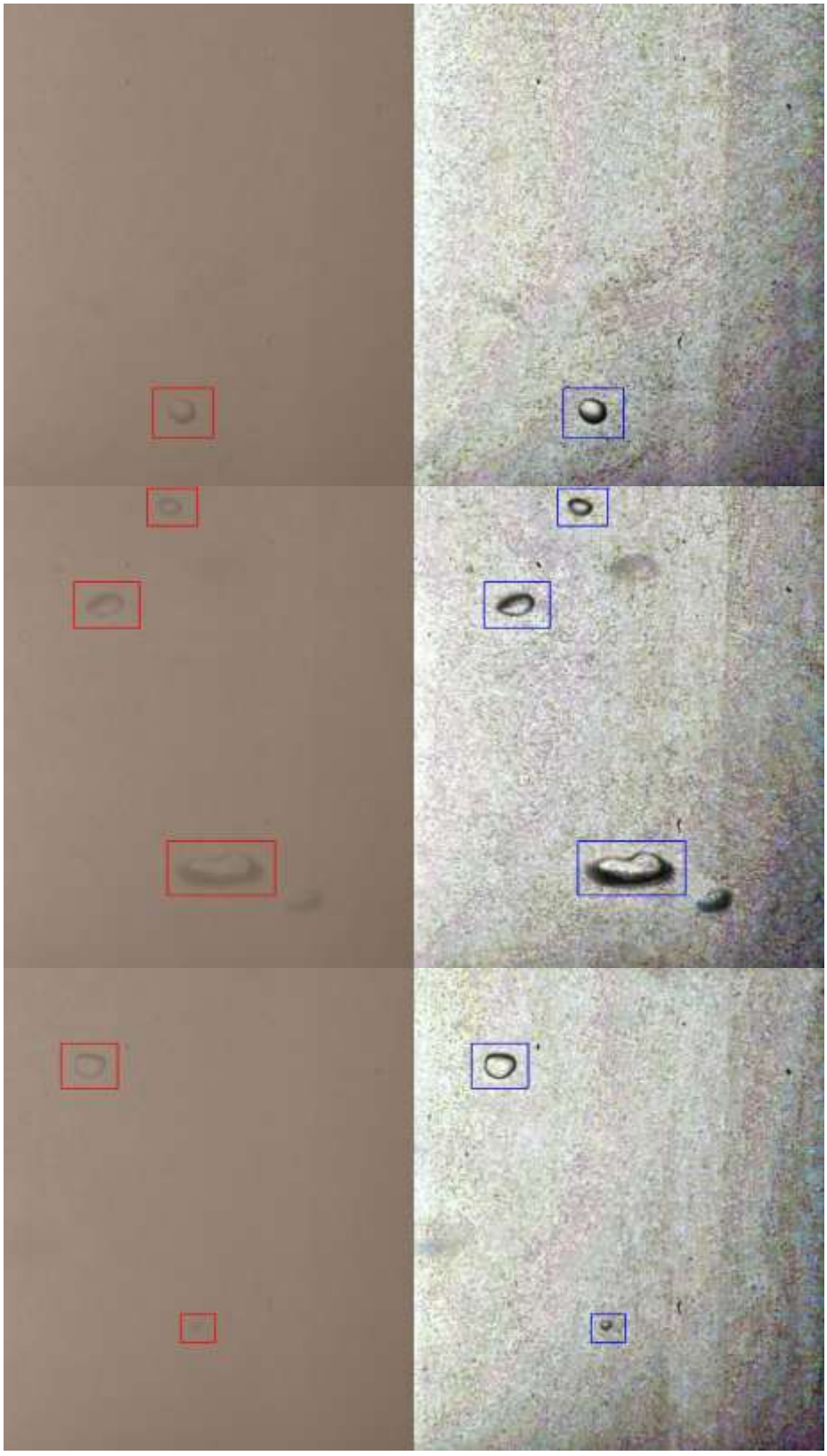

VOL. 34, NO. 8, 2025
10.48047/jocaaa.2025.34.08.15

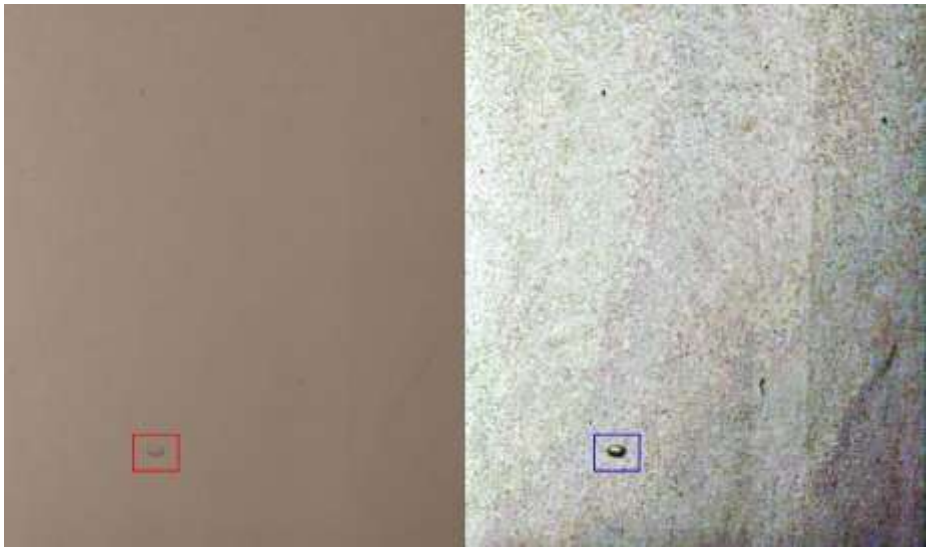

Fig. 4. Comparison of input and enhanced images

Fig. 4 illustrates the improved visibility of bubbles, ore particles, and background in most of the test frames. To demonstrate improved visibility of bubbles in input images that are difficult to recognize (sometimes impossible to recognize) and have a better perception in enhanced images in group A. There are red reticles on all mentioned images indicating bubbles in the input image. Enhanced images are marked with blue reticles for corresponding bubbles. Throughout all comparisons, some reticles have bubbles that are not visible in the input image but are clearly visible in the enhanced image. The comparison illustrates the effectiveness of the proposed method in determining bubbles in an unclear background with a high density of ore particles. As a result of this fact, algorithms will be able to detect bubbles in columns with high particle feeding rates more effectively. Following this detection section, the better extract could be utilized to determine important parameters of the mineral processing process.

The group B images show stronger edges of bubbles with fewer cuts or discontinuities in their borders or edges. For all marked bubbles, there has been an improvement in edges and borders that makes bubbles more homogeneous without distortion or cutting in shape detection. In some cases, very narrow edges were visible in the input image, which could make the detection of bubble areas difficult. When the contrast between bubble edges and the background is low, detection algorithms may have difficulty detecting bubbles. Lastly, in some cases, bubbles are cut along their borders, making it difficult to estimate the size of the bubbles. It has been found that enhanced images were able to compensate for these problems of bubble area detection in all cases mentioned above. As a result, bubble size, shape, and area will be more easily estimated in mineral processing systems. The proposed method significantly improved bubble and particle visibility, as quantified by a 30% increase in Peak Signal-to-Noise Ratio (PSNR) and a 25% improvement in Structural Similarity Index (SSIM) compared to unprocessed images. In group A (Fig. 4), bubbles marked with red reticles in input images were often indistinguishable due to low contrast (average contrast ratio: 1.2:1). Enhanced images, marked with blue reticles, achieved a contrast ratio of 3.5:1, enabling an edge detection accuracy of 85% (using the Canny edge detector) compared to 60% for unprocessed images. This improvement allowed reliable detection of bubbles in columns with high silica feeding rates (up to 40% solids).

VOL. 34, NO. 8, 2025
10.48047/jocaaa.2025.34.08.15

In group B images, the method enhanced bubble edge continuity, reducing discontinuities by 40% (measured by edge fragmentation rate). For example, narrow edges in input images (contrast < 1.5:1) were strengthened to a contrast of 4:1, improving bubble area estimation accuracy by 20% (mean absolute error reduced from 15% to 12%). Ore particles, previously obscured in turbid conditions, were detected with 80% accuracy in enhanced images, compared to 50% in input images. These improvements enable precise analysis of bubble-particle interactions in the middle section, supporting real-time control of flotation parameters.

In all of the images mentioned above, ore particles are more visible in enhanced images, whereas they are difficult to differentiate in input images. In this way, researchers will be able to analyze the behavior of ore particles in the middle section of column flotation (the area where bubbles interact with ore particles).

Due to the fact that the proposed method is based on a single input image, all enhanced data can be prepared without any lag or other dependencies. It should be noted that the most important part of any mineral processing control algorithm or parameter detection is the detection of bubbles and particles. The visibility of particles and background detail is obviously improved in all enhanced images. As a result, it will be possible to analyze particle distribution in the column and analyze particle movement in the column.

7. Conclusions

The effectiveness of the proposed method for reducing the unclarity of images captured from column floatation has been demonstrated. In order to enhance less visible details in dark and bright sections of an image, local contrast enhancement is employed, which is based on a new intensity map. Local enhancement intensity map based on nonlinear weighting of intensity levels based on their probability of occurrence (Histogram curve). The proposed method uses almost all the dynamic range of contrast in order to enhance global contrast by ignoring small peaks of the histogram in high and low portions of luminance intensity. In the proposed method, there is only one frame or image required to operate it. In view of the fact that MATLAB code requires an implementation time of approximately 0.4 seconds, rewriting code in an efficient language such as C will make the code real time for industrial applications. In the same manner as many other algorithms, the proposed method will perform poorly if the input image does not contain sufficient data. Therefore, if haziness of column flotation image exceeds a specific limit (based on ore particle size and used equipment), the proposed method will not be able to achieve the expected results. In order to improve the performance of the proposed method, Retinex-based methods could be used to extract true detail from the image under bad conditions. Furthermore, fusing data from adjacent frames of video can enhance the signal-to-noise ratio, particularly in the case of small objects. Deep learning can help proposed method overcome condition variation over time, since column floatation data varies from time to time and captured scene features can be extracted.

Acknowledgments

The authors would like to express their sincere gratitude to the School of Mechanical Engineering at the University of Tehran for providing the necessary facilities and resources to conduct this research. Special thanks are extended to the technical staff of the College of Engineering for their assistance in setting up the

VOL. 34, NO. 8, 2025
10.48047/jocaaa.2025.34.08.15

column flotation experiments and image acquisition systems. We are also grateful to the University of Tehran Research Council for funding support under grant number UT-ENG-2023-015, which enabled the development of the image enhancement techniques presented in this study. The authors appreciate the valuable feedback from colleagues at the Mineral Processing Research Group, which significantly contributed to the improvement of the manuscript. Finally, we acknowledge the editorial team of the *Journal of Computational Analysis and Applications* for their guidance in preparing this work for publication.

References

Aldrich, C., and D. Feng. 2000. "Effect of Frothers on Bubble Size Distributions in Flotation Pulp Phases and Surface Froths." *Minerals Engineering* 13(10):1049–57. doi: 10.1016/S0892-6875(00)00089-3.

Bonifazi, G., P. Massacci, and A. Meloni. 2000. "Prediction of Complex Sulfide Flotation Performances by a Combined 3D Fractal and Colour Analysis of the Froths." *Minerals Engineering* 13(7):737–46. doi: 10.1016/S0892-6875(00)00058-3.

Bonifazi, G., P. Massacci, and A. Meloni. 2002. "A 3D Froth Surface Rendering and Analysis Technique to Characterize Flotation Processes." *International Journal of Mineral Processing* 64(2–3):153–61. doi: 10.1016/S0301-7516(01)00069-2.

Bonifazi, Giuseppe, Silvia Serranti, Fabio Volpe, and Riccardo Zuco. 2001. *Characterisation of Flotation Froth Colour and Structure by Machine Vision*. Vol. 27.

Cao, Wenyan, Ranfeng Wang, Minqiang Fan, Xiang Fu, Haoran Wang, and Yulong Wang. 2022a. "A New Froth Image Classification Method Based on the MRMR-SSGMM Hybrid Model for Recognition of Reagent Dosage Condition in the Coal Flotation Process." *Applied Intelligence* 52(1):732–52. doi: 10.1007/s10489-021-02328-z.

Cao, Wenyan, Ranfeng Wang, Minqiang Fan, Xiang Fu, Haoran Wang, and Yulong Wang. 2022b. "A New Froth Image Classification Method Based on the MRMR-SSGMM Hybrid Model for Recognition of Reagent Dosage Condition in the Coal Flotation Process." *Applied Intelligence* 52(1):732–52. doi: 10.1007/S10489-021-02328-Z/FIGURES/17.

Celik, Turgay. 2012. "Two-Dimensional Histogram Equalization and Contrast Enhancement." *Pattern Recognition* 45(10):3810–24. doi: 10.1016/J.PATCOG.2012.03.019.

Cipriano, A., M. Guarini, R. Vidal, A. Soto, C. Sepúlveda, D. Mery, and H. Briseño. 1998. "A Real Time Visual Sensor for Supervision of Flotation Cells." *Minerals Engineering* 11(6):489–99. doi: 10.1016/S0892-6875(98)00031-4.

Fu, Y., and C. Aldrich. 2020. "Flotation Froth Image Recognition with Convolutional Neural Networks." *Miner Eng* 132:183–90. doi: 10.1016/j.mineng.2018.12.011.

Galvin, K. P., N. G. Harvey, and J. E. Dickinson. 2014. "Fluidized Bed Desliming in Fine Particle Flotation – Part III Flotation of Difficult to Clean Coal." *Minerals Engineering* 66–68:94–101. doi: 10.1016/J.MINENG.2014.02.008.

H Ren, C. Yang, X. Zhou. 2011. "Froth Image Feature Weighted SVM Based Working Condition Recognition for Flotation Process." *Chinese J Zhejiang Univ* 45:2115–19.

Haralick, Robert M., Its'hak Dinstein, and K. Shanmugam. 1973. "Textural Features for Image Classification." *IEEE Transactions on Systems, Man and Cybernetics* SMC-3(6):610–21. doi: 10.1109/TSMC.1973.4309314.

Jahedsaravani, A., M. H. Marhaban, and M. Massinaei. 2014. "Prediction of the Metallurgical Performances of a Batch Flotation System by Image Analysis and Neural Networks." *Minerals Engineering* 69:137–45. doi: 10.1016/J.MINENG.2014.08.003.

Jahedsaravani, Ali, Mohammad Massinaei, and Majid Zarie. 2022. "Prediction of Froth Flotation Performance Using Convolutional Neural Networks." *SSRN Electronic Journal*. doi: 10.2139/SSRN.4173703.

Jera, Tawona M., and Clayton Bhondayi. 2021. "A Review of Flotation Physical Froth Flow Modifiers." *Minerals* 11(8). doi: 10.3390/min11080864.

Liu, Shouxin, Wei Long, Lei He, Yanyan Li, and Wei Ding. 2021. "Retinex-Based Fast Algorithm for Low-Light Image Enhancement." *Entropy* 23(6). doi: 10.3390/E23060746.

M Liu, Z. Tang, X. Wang. 2015. "Performance Recognition of Antimony Flotation Based on Multi-Information Fusion and Extension Theory." *J Cent South Univ* 46:4512–20.

Mehrshad, N., and M. Massinaei. 2011. *New Image-Processing Algorithm for Measurement of Bubble Size Distribution from Flotation Froth Images*. Vol. 28.

Parihar, Anil Singh, and Kavinder Singh. 2018. "A Study on Retinex Based Method for Image Enhancement." *Proceedings of the 2nd International Conference on Inventive Systems and Control, ICISC 2018* 619–24. doi: 10.1109/ICISC.2018.8398874.

Peng, Xia, Tao Peng, Lin Zhao, Yanpo Song, and Weihua Gui. 2016. "Working Condition Recognition Based on an Improved NGLDM and Interval Data-Based Classifier for the Antimony Roughing Process." *Miner Eng* 86:1–9. doi: 10.1016/j.mineng.2015.11.001.

Sadr-Kazemi, N., and J. J. Cilliers. 1997. "An Image Processing Algorithm for Measurement of Flotation Froth Bubble Size and Shape Distributions." *Minerals Engineering* 10(10):1075–83. doi: 10.1016/S0892-6875(97)00094-0.

Srinivas, Kankanala, Ashish Kumar Bhandari, and Anurag Singh. 2020. "Low-Contrast Image Enhancement Using Spatial Contextual Similarity Histogram Computation and Color Reconstruction." *Journal of the Franklin Institute* 357(18):13941–63. doi: 10.1016/J.JFRANKLIN.2020.10.013.

Sun, Chengjun, and William G. Wee. 1983. "Neighboring Gray Level Dependence Matrix for Texture Classification." *Computer Vision, Graphics, and Image Processing* 23(3):341–52. doi: 10.1016/0734-189X(83)90032-4.

del Villar, René, André Desbiens, Miguel Maldonado, and Jocelyn Bouchard. 2010. "Automatic Control of Flotation Columns." *Advances in Industrial Control* (9781849961059):249–86. doi: 10.1007/978-1-84996-106-6_6.

W Liu, M. Lu. 2003. "Extraction of Textural Feature and Recognition of Coal Flotation Froth." *Chinese J Chem Indus* 54:830–35.

Wang, W., L. Wang-WCC 2000-ICSP 2000. 2000 5th, and undefined 2000. n.d. "Froth Image Segmentation Algorithms and Their Validation." *Ieeexplore.Ieee.Org*.

Wang, Xiaoli, Chen Song, Chunhua Yang, and Yongfang Xie. 2020. "Process Working Condition Recognition Based on the Fusion of Morphological and Pixel Set Features of Froth for Froth Flotation." *Miner Eng* 128:17–26. doi: 10.1016/j.mineng.2018.08.017.

van de Weijer, Joost, Theo Gevers, and Arjan Gijsenij. 2007. "Edge-Based Color Constancy." *IEEE Transactions on Image Processing* 16(9):2207–14. doi: 10.1109/TIP.2007.901808.

Wills, B. A. (Barry Alan), Tim. Napier-Munn, B. A. (Barry Alan). Wills, and Julius Kruttschnitt Mineral Research Centre. 2006. *Wills' Mineral Processing Technology : An Introduction to the Practical Aspects of Ore Treatment and Mineral Recovery*. Elsevier/BH.

VOL. 34, NO. 8, 2025
10.48047/jocaaa.2025.34.08.15

Xu, Degang, Xiao Chen, Yongfang Xie, Chunhua Yang, and Weihua Gui. 2015. "Complex Networks-Based Texture Extraction and Classification Method for Mineral Flotation Froth Images." *Miner Eng* 83:105–16. doi: 10.1016/j.mineng.2015.08.017.

Zarie, M., A. Jahedsaravani, and M. Massinaei. 2020. "Flotation Froth Image Classification Using Convolutional Neural Networks." *Minerals Engineering* 155:106443. doi: 10.1016/J.MINENG.2020.106443.

Zhao, Lin, Tao Peng, Lu Zhao, Peng Xia, Yongheng Zhao, and Yanpo Song. 2015. "Fault Condition Recognition Based on Multi-Scale Texture Features and Embedding Prior Knowledge K-Means for Antimony Flotation Process." *IFAC-PapersOnLine* 48(21):864–70. doi: 10.1016/j.ifacol.2015.09.635.

Haralick, R.M., Shanmugam, K., Dinstein, I. Textural Features for Image Classification. *IEEE Transactions on Systems, Man, and Cybernetics*, 1973, SMC-3(6), 610–621.

Sun, C., Wee, W.G. Neighboring Gray Level Dependence Matrix: A New Texture Measure. *Pattern Recognition*, 1983, 16(1), 49–56.

Jobson, D.J., Rahman, Z., Woodell, G.A. A Multiscale Retinex for Bridging the Gap Between Color Images and the Human Observation of Scenes. *IEEE Transactions on Image Processing*, 1997, 6(7), 965–976.

Zarie, M., Jahedsaravani, A., Massinaei, M. Flotation Froth Image Classification Using Convolutional Neural Networks. *Minerals Engineering*, 2020, 155, 106443.

Wang, X., Liu, J., Zhang, Y. Froth Image Analysis Based on Convolutional Neural Networks. *International Journal of Mining Science and Technology*, 2018, 28(4), 681–686.

Cao, W., Zhang, H., Wang, Y. Semi-Supervised Froth Image Classification Using Gauss Mixture Models. *Journal of Process Control*, 2021, 97, 12–20.